Current Applied Physics 13 (2013) 224–227

Contents lists available at SciVerse ScienceDirect

Current Applied Physics

journal homepage: www.elsevier.com/locate/cap

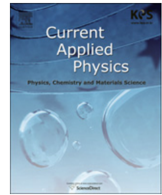

The effect of $In_xGa_{1-x}N$ back-barriers on the dislocation densities in $Al_{0.31}Ga_{0.69}N/AlN/GaN/In_xGa_{1-x}N/GaN$ heterostructures ($0.05 \le x \le 0.14$)

B. Sarikavak-Lisesivdin [a,*], S.B. Lisesivdin [a], E. Ozbay [b,c,d]

[a] Gazi University, Faculty of Science, Department of Physics, 06500 Teknikokullar, Ankara, Turkey
[b] Bilkent University, Nanotechnology Research Center, 06800 Bilkent, Turkey
[c] Bilkent University, Department of Physics, 06800 Bilkent, Turkey
[d] Bilkent University, Department of Electrical and Electronics Engineering, 06800 Bilkent, Turkey

ARTICLE INFO

Article history:
Received 12 June 2012
Accepted 13 July 2012
Available online 22 July 2012

Keywords:
InGaN back-barrier
MOCVD
XRD
Defect analyses

ABSTRACT

$Al_{0.31}Ga_{0.69}N/AlN/GaN/In_xGa_{1-x}N/GaN$ heterostructures grown with the metal-organic chemical vapor deposition (MOCVD) technique with different $In_xGa_{1-x}N$ back-barriers with In mole fractions of $0.05 \le x \le 0.14$ were investigated by using XRD measurements. Screw, edge, and total dislocations, In mole fraction of back-barriers, Al mole fraction, and the thicknesses of front-barriers and lattice parameters were calculated. Mixed state dislocations with both edge and screw type dislocations were observed. The effects of the In mole fraction difference in the back-barrier and the effect of the thickness of front-barrier on crystal quality are discussed. With the increasing In mole fraction, an increasing dislocation trend is observed that may be due to the growth temperature difference between ultrathin $In_xGa_{1-x}N$ back-barrier and the surrounding layers.

© 2012 Elsevier B.V. All rights reserved.

1. Introduction

Nitride based high electron mobility transistors (HEMTs) are one of the most actively investigated device structures over the last decade due to large breakdown field and strong spontaneous and piezoelectric polarization fields that result in possible applications in military and high power usage [1–4]. For obtaining higher device performance with these heterostructures, different channel, barrier, and buffer alternatives were proposed in terms of different materials, additional layers and thicknesses, and used for years after the first proposed AlGaN/GaN type heterostructures [5]. Channel modulation doped double heterostructures [6], AlGaN/InGaN/AlGaN double-heterostructures [7], AlGaN/AlN/GaN with thin AlN interlayer [8], highly polar AlInN/GaN structures [9], and ultrathin barrier structures [10] can be shown as an important engineering milestones for nitride based HEMT history.

One of the reported device performance increments is due to the use of an ultrathin layer of $In_xGa_{1-x}N$ at GaN buffer [11,12]. With the inserting of an ultrathin $In_xGa_{1-x}N$ layer, the conduction band of the GaN buffer is raised with respect to the GaN channel in order to increase the confinement of the electrons. This results in an effective conduction band discontinuity of approximately a few hundred meVs with a 1 nm thick ultrathin back-barrier of $In_xGa_{1-x}N$. However, because the $In_xGa_{1-x}N$ layers are grown with high dislocations at higher growth temperatures ($T > 1000$ °C), lower temperatures must be used, and even a change in temperature may lead to a formation of embedded $In_xGa_{1-x}N$ or even InN quantum dots around the designated layers [13].

Therefore, it is very important to understand the formation of dislocations with the insertion of a low-temperature grown $In_xGa_{1-x}N$ back-barrier layer to crystalline quality, which is highly related with the device performance because the two-dimensional electron gas (2DEG) is just populated above this $In_xGa_{1-x}N$ back-barrier layer.

In this work, we investigated the crystalline properties in $Al_{0.31}Ga_{0.69}N/AlN/GaN/In_xGa_{1-x}N/GaN$ double heterostructures with In mole fractions ($x = 0$–0.14) using X-ray diffraction (XRD) methods.

2. Experimental details

$Al_{0.25}Ga_{0.75}N/AlN/GaN/In_xGa_{1-x}N/GaN$ HEMT samples that were studied in this study were grown on identical c-face (0001) sapphire substrates in a vertical low-pressure metal-organic chemical vapor deposition (MOCVD) system. Before epitaxial growth, the substrates were annealed at 1050 °C for 15 min in order to maintain surface cleaning. After desorption of the unwanted materials from the sapphire surface, the growth was started with a 15 nm AlN nucleation layer at a relatively low temperature (LT) of

* Corresponding author. Tel.: +90 3122021266.
E-mail address: beyzas@gmail.com (B. Sarikavak-Lisesivdin).

1567-1739/$ – see front matter © 2012 Elsevier B.V. All rights reserved.
http://dx.doi.org/10.1016/j.cap.2012.07.012

550 °C. Then, a nearly 0.5 μm AlN buffer layer was grown at a relatively high temperature (HT) of 1150 °C. Buffer layers are completed with growing a 1.3 μm thick nominally undoped GaN buffer layer at 1050 °C. After the buffer, each sample has a different $In_xGa_{1-x}N$ back-barrier layer that was grown at a temperature range of 795–740 °C, resulting in In mole fractions between 0.05 and 0.14, respectively. After the back-barrier layer, a 10 nm LT GaN channel layer and a ~1 nm HT AlN interlayer were grown. The interlayer is a highly used layer in the literature in order to reduce the alloy disorder scattering [8,10]. Then, a nearly 20 nm HT $Al_{0.31}Ga_{0.69}N$ barrier layer and 3 nm HT GaN cap layer were deposited on the inter-layer to finalize the growth. All the layers were grown undoped. The layer structure of the samples is shown in Fig. 1. The layer thicknesses and Al mole fractions of the front-barrier layer, In mole fractions of back-barrier layers, and lattice parameters were determined by using the XRD technique.

The XRD measurements were performed by Rigaku SmartLab diffractometer equipped with a four crystal Ge (220) monochromator for the $CuK_{\alpha 1}$ X-ray beam ($\lambda = 1.5406$ Å). The rocking curves of the samples were measured by $\omega - 2\theta$ scan (where ω and 2θ are the angles of the sample and detector relative to the incident X-ray beam). Asymmetric and symmetric scans measured by XRD for comparing the relations tilt and twist the properties of layers.

3. Results and discussion

In order to unroll the importance of $In_xGa_{1-x}N$ back-barriers, we solved the 1-dimensional nonlinear Schrödinger–Poisson equations self-consistently for the studied HEMT structures [14]. The steps of the simulation procedure, for systems like this study's, were given elsewhere [15]. The results are shown in Fig. 2. As shown in the figure, with increasing In mole fraction, the conduction band offset at the back-barrier layer and a part of the channel layer near the back-barrier layer, decreases. However, the band offset at the buffer near the back-barrier layer increases in contrast to the situation observed at the back-barrier layer channel layer and a part of the channel layer near the back-barrier layer. Therefore, increasing In mole fraction results in band discontinuity and a better confinement in the channel, which can be seen in the inset of Fig. 2, where a carrier increase is calculated at a part of the channel layer near the back-barrier layer. However, with different growth temperatures, these back-barriers may induce strain relaxation due to high dislocation densities on upper layers, which may result in bad device performance. The band discontinuity for the $x = 0.05$, 0.10, and 0.14 cases are calculated as 152, 250, and 345 meV, respectively.

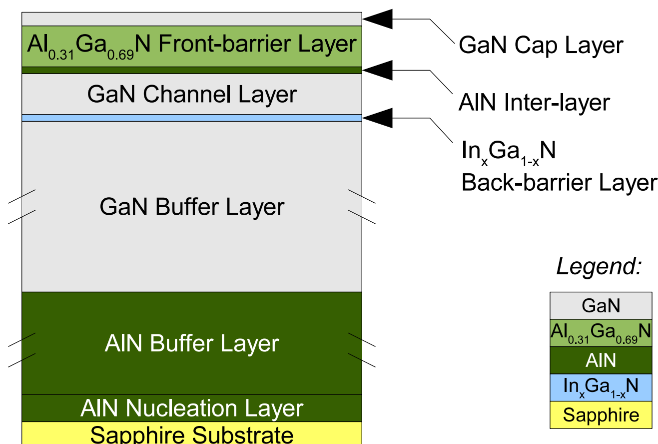

Fig. 1. The layer structure of the studied samples.

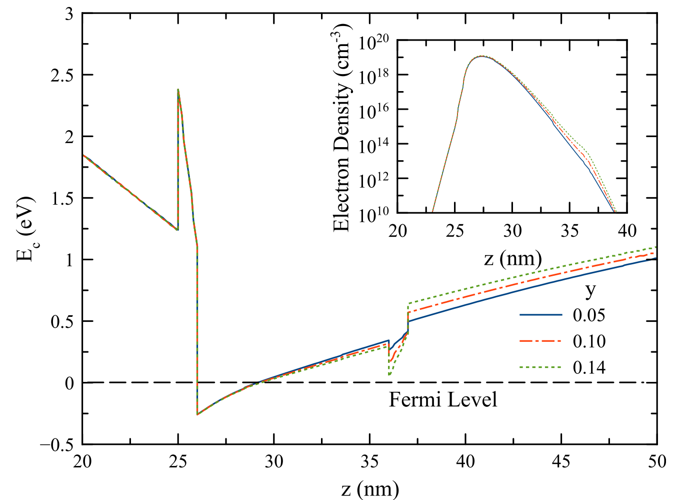

Fig. 2. Conduction band profile for the studied samples where $y = 0.05$ (blue full line), $y = 0.10$ (red dash-dots), $y = 0.14$ (green dots) and Fermi level (black dashs) Inset: electron density probability distribution in pseudotriangular quantum well formed near the AlN inter-layer and at the GaN channel layer. (For interpretation of the references to color in this figure legend, the reader is referred to the web version of this article.)

By using XRD rocking curve data, the structural quality of samples was determined from the full width at half maximum (FWHM) values of clearly resolved Pendellösung fringes. Fig. 3 shows (0002) reflections of scans of GaN, $In_xGa_{1-x}N$, $Al_{0.31}Ga_{0.69}N$ and AlN fringes for four different samples. Sample 1688 has the best separated peaks. The $In_xGa_{1-x}N$ peak must be seen as a shoulder of GaN peak. However, due to the thickness of the $In_xGa_{1-x}N$ layer, the peak of the $In_xGa_{1-x}N$ layer cannot be observed clearly from the $\omega - 2\theta$ scan.

Pendellösung fringes observed from the experimental result shows no rugosity at the interfaces and a very good correlation between the measured and expected layer thicknesses from the growth rate. The large FWHM of the thick GaN buffer layer integrates both the effect of the GaN channel layer and the mosaicity induced by the grown dislocations [11,12]. The measured rocking curves of the $\omega - 2\theta$ scans are compared for different reflections. For each reflection, we fitted the results by the pseudo-Voigt function as shown in Fig. 4. The broadening of the rocking curve peaks gives information about the dislocation densities of the layered structure. In Fig. 4, example peaks of symmetric and

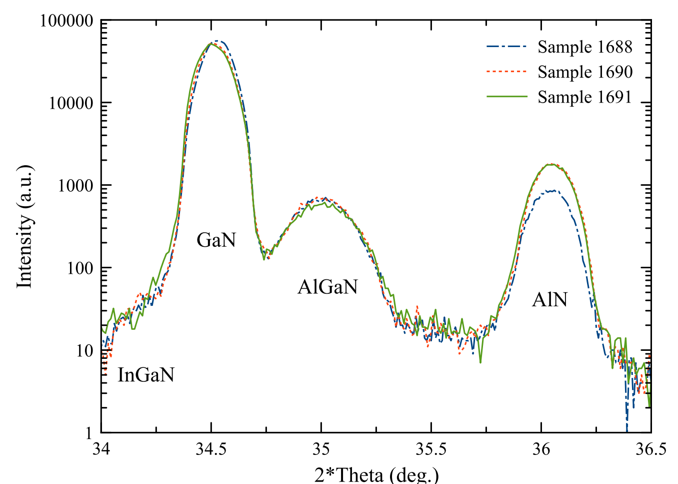

Fig. 3. The $\omega - 2\theta$ scans for the Samples 1688, 1690, and 1691.

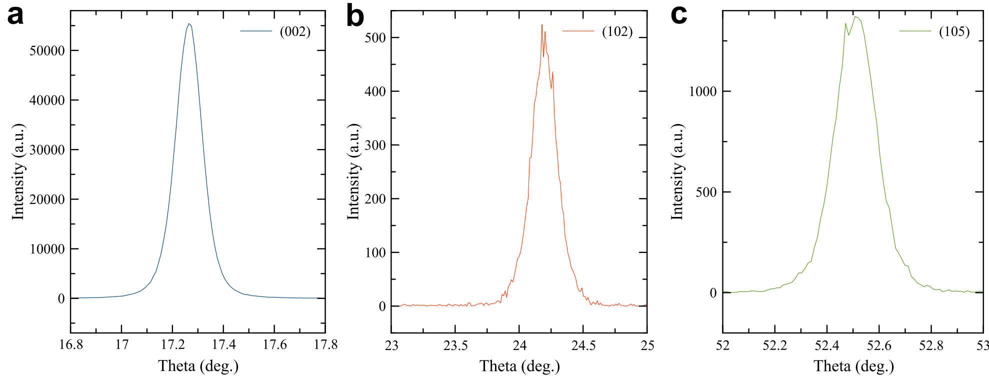

Fig. 4. Peaks of symmetric and asymmetric reflections of GaN layer for (a) (002), (b) (102) and (c) (105) of Sample 1688.

asymmetric reflections are shown for sample 1688. As shown in the figure, (002) direction has the sharpest and narrowest peaks with respect to asymmetric reflections as usual.

The interplanar spacing, d, of the ($hkil$) plane for a hexagonal unit cell is given as,

$$\frac{1}{d_{hkl}^2} = \frac{4}{3}\frac{h^2+k^2+hk}{a^2} + \frac{l^2}{c^2}, \quad (1)$$

where a and c are the lattice parameters.

Lattice constant, c can be calculated by using (0001) symmetric XRD reflections. (0001) is the growth direction of $In_xGa_{1-x}N$. Determining of the lattice constant is easier experimentally.

From Bragg's law, the lattice constant, c_0, for any allowed (0001) reflection can be derived from Bragg's law [11],

$$c_0 = l\lambda/(2\sin\theta), \quad (2)$$

$$x = \frac{(c_0 - c_{GaN})}{(c_{InN} - c_{GaN})}. \quad (3)$$

In mole fraction can be determined by Eq. (2) and Eq. (3) with the peak position, which may be found from the fitting of $In_xGa_{1-x}N$ peak of the measured rocking curve of $\omega - 2\theta$ scan.

Because of that, there is a single $Al_{0.31}Ga_{0.69}N$ layer in the studied samples and it is near the – center of interest – GaN channel, and dislocation densities are calculated for this $Al_{0.31}Ga_{0.69}N$ layer. Screw, edge, and total dislocations at the $Al_{0.31}Ga_{0.69}N$ front-barrier calculated by using symmetric and asymmetric FWHM of the $Al_{0.31}Ga_{0.69}N$ layer's rocking curve for the samples as,

$$N_{screw} = \frac{FWHM_{(002)}^2}{9b_{screw}^2}, \quad (4)$$

$$N_{edge} = \frac{FWHM_{(102)}^2}{9b_{edge}^2}, \quad (5)$$

$$N_{dis} = N_{screw} + N_{edge}, \quad (6)$$

Lattice parameters c_0 and In mole fractions x of back-barrier layers, Al mole fractions and thicknesses of front-barrier layers, N_{screw}, N_{edge} and N_{dis} values are listed in Table 1. According to the results, edge dislocations seem to be dominating the samples with respect to screw dislocations. The thickness of the barrier layer is $t = \lambda/2\delta\cos\theta_B$ where δ is FWHM and θ_B is the angular position of the barrier layer.

In Fig. 5, the FWHM values of (102) rocking curves are shown versus the (002) rocking curves for the sample with different $In_xGa_{1-x}N$ back-barriers with different In mole fractions. A nearly linear dependence is observed for the studied samples. Fig. 5 suggests increasing edge dislocation densities with increasing screw dislocation density, where the edge dislocation density is much higher than the screw dislocation density for all the samples. This result, which means a correlation between tilt and twist, is known and is in agreement with the literature [16–19]. A simultaneous increase in both edge and screw dislocation densities can be explained by the growth condition difference (in our case, the In mole fraction of back-barriers), favoring a simultaneous increase in

Table 1
Lattice parameters c_0 and In mole fractions x of back-barriers, Al mole fractions and the thicknesses of the front-barrier layers, N_{screw}, N_{edge} and N_{dis} values.

	Samples		
	1688	1690	1691
c_0 of $In_xGa_{1-x}N$ barrier layer (Å)	5.239	5.211	5.258
In mole fraction (x)	0.105	0.049	0.140
Al mole fraction	0.309	0.311	0.310
Thickness of the AlGaN barrier layer	21.13	22.68	18.81
N_{screw} ($\times 10^8$ cm^{-2})	4.762	5.852	7.694
N_{edge} ($\times 10^9$ cm^{-2})	4.521	5.678	9.075
N_{dis} ($\times 10^9$ cm^{-2})	4.997	6.263	9.844

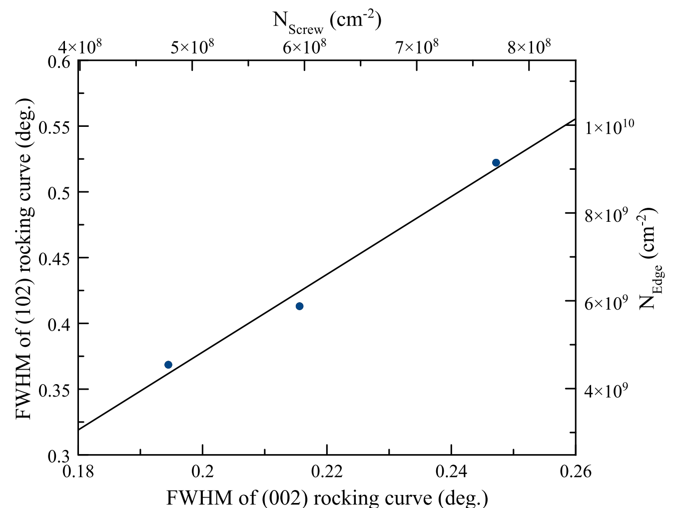

Fig. 5. FWHM values of the (102) rocking curve versus (002) rocking curve for the sample with $In_xGa_{1-x}N$ back-barriers with different In mole fractions. Line is a linear fit.

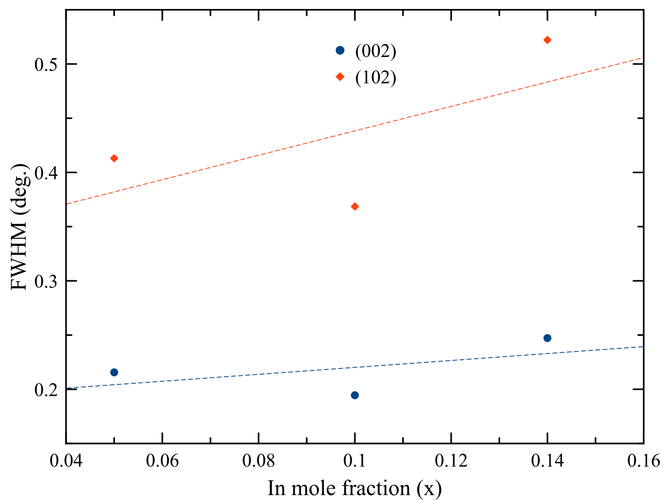

Fig. 6. Rocking curve FWHM versus In mole fraction (x) of $In_xGa_{1-x}N$ back-barriers. Lines are linear fits.

tilt and twist [18]. In addition, the creation of mixed dislocations can be suggested in our case.

Fig. 6 shows the In mole fraction dependent FWHM values for both symmetric and asymmetric peaks of studied samples. With the increasing In mole fraction, in which the strain will be increased and, therefore, an increment in the FWHM values is expected. However, from the In mole fraction of $x = 0.05-0.10$, a decrement is observed. This behavior is unexpected. This unexpected behavior can be understood when the calculated $Al_{0.31}Ga_{0.69}N$ front-barrier parameters are investigated. For a simple two-layer approximation, the critical thickness before any strain relaxation occurring can be calculated with,

$$t_c \approx \frac{b_e}{2\varepsilon_x}. \tag{7}$$

Here, b_e is the Burger vector ($b_e = 0.31825$ nm) and ε_x is the biaxial strain. With the knowledge of the Al mole fraction of 0.31 for front-barriers, and with Eq. (7), critical thickness can be found as nearly 19 nm for the studied samples. This value is below the thickness of the front-barrier of Sample 1691. However, the thicknesses of the front-barriers of Samples 1688 and 1690 are greater than this value, which means strain relaxation may occur in these samples. Sample 1690 has the biggest front-barrier thickness and the Al mole fraction, in which we may conclude that strain relaxation has a major impact on Sample 1690's crystalline properties. And we can conclude that front-barriers effects on crystalline properties seem to be dominant with respect to the back-barrier due to the larger lattice mismatch of AlN/GaN systems with respect to InN/GaN systems.

In Fig. 6, fits show an increasing trend of FWHM change due to In mole fraction, which shows an important negative effect of the increment of the In mole fraction to crystalline quality.

4. Conclusions

We studied the crystalline properties of $Al_{0.31}Ga_{0.69}N$/AlN/GaN/$In_xGa_{1-x}N$/GaN heterostructures with different In mole fractions of $x = 0.05-0.14$ by using XRD measurements. Screw, edge, and total dislocations, In mole fraction of back-barriers, Al mole fraction and thicknesses of front-barriers, and lattice parameters were calculated. Mixed state dislocations with both edge and screw type dislocations were observed. Edge and screw dislocations seem to increase linearly, which means the growth condition difference favors both tilt and twist. In addition to the effects of the In mole fraction difference in the back-barrier, the effect of the thickness of front-barrier is also discussed as its effect is dominant with respect to the effect of the In mole fraction difference in the back-barrier.

Quality $In_xGa_{1-x}N$ layers are known to be grown in lower temperatures. In our samples' growth, ultrathin $In_xGa_{1-x}N$ layers were grown at lower temperatures instead of the higher temperature grown surrounding layers. Therefore, with the increasing In mole fraction, this temperature difference becomes more effective and an increasing dislocation trend was observed in our samples.

Acknowledgments

This work is supported by the State Planning Organization of Turkey under Grant No. 2001K120590, by the European Union under the projects EU-PHOME and EU-ECONAM, and TUBITAK under the Project Nos. 106E198, 107A004, and 107A012. One of the authors (Ekmel Ozbay) acknowledges partial support from the Turkish Academy of Sciences. We would like to thank the NANOTAM engineers for their help.

References

[1] W. Nagy, J. Brown, R. Borges, S. Singhal, IEEE Trans. Microw. Theory Tech. 51 (2003) 660.
[2] M. Feng, S. Shyh-Chiang, D.C. Caruth, J.J. Huang, Proc. IEEE 92 (2004) 354.
[3] A. Yildiz, S.B. Lisesivdin, P. Tasli, E. Ozbay, M. Kasap, Curr. Appl. Phys. 10 (2010) 838.
[4] T.K. Kim, S.K. Shim, S.S. Yang, J.K. Son, Y.K. Hong, G.M. Yang, Curr. Appl. Phys. 7 (2007) 469.
[5] M. Asif Khan, J.N. Kuznia, J.M. Van Hove, N. Pan, J. Carter, Appl. Phys. Lett. 60 (1992) 3027.
[6] Z. Fan, C. Lu, A.E. Botchkarev, H. Tang, A. Salvador, O. Aktas, W. Kim, H. Morkoc, Electron. Lett. 33 (1997) 814.
[7] N. Maeda, T. Saitoh, K. Tsubaki, T. Nishida, N. Kobayashi, Jpn. J. Appl. Phys. 38 (1999) L799.
[8] I.P. Smorchkova, L. Chen, T. Mates, L. Shen, S. Heikman, B. Moran, S. Keller, S.P. DenBaars, J.S. Speck, U.K. Mishra, J. Appl. Phys. 90 (2001) 3998.
[9] J. Kuzmík, IEEE Electron. Device Lett. 22 (2001) 510.
[10] C. Ostermaier, G. Pozzovivo, J.-F. Carlin, B. Basnar, W. Schrenk, Y. Douvry, C. Gaquiere, J.-C. DeJaeger, K. Cico, K. Fröhlich, M. Gonschorek, N. Grandjean, G. Strasser, D. Pogany, J. Kuzmík, IEEE Electron. Device Lett. 30 (2009) 1030.
[11] T. Palacios, A. Chakraborty, S. Heikman, S. Keller, S.P. DenBaars, U.K. Mishra, IEEE Electron. Device Lett. 27 (2006) 13.
[12] T. Palacios, Y. Dora, A. Chakraborty, C. Sanabria, S. Keller, S.P. DenBaars, U.K. Mishra, Phys. Stat. Sol. (A) 203 (2006) 1845.
[13] Y.S. Lin, K.J. Ma, C. Hsu, Y.Y. Chung, C.W. Liu, S.W. Feng, Y.C. Cheng, M.H. Mao, C.C. Yang, H.W. Chuang, C.T. Kuo, J.S. Tsang, T.E. Weirich, Appl. Phys. Lett. 80 (2002) 2571.
[14] S. Birner, S. Hackenbuchner, M. Sabathil, G. Zandler, J.A. Majewski, T. Andlauer, T. Zibold, R. Morschl, A. Trellakis, P. Vogl, Acta Phys. Pol. A 110 (2006) 111.
[15] P. Tasli, B. Sarikavak, G. Atmaca, K. Elibol, A.F. Kuloglu, S.B. Lisesivdin, Phys. B 405 (2010) 4020.
[16] T. Matsuoka, T. Sasaki, A. Katsui, Optoelectronics 5 (1990) 53.
[17] M.K. Ozturk, Y. Hongbo, B. Sarikavak, S. Korcak, S. Ozcelik, E. Ozbay, J. Mater. Sci. Mater. Electron. 21 (2010) 185.
[18] H. Heinke, V. Kirchner, S. Einfeldt, D. Hommel, Appl. Phys. Lett. 77 (2000) 2145.
[19] W. Qian, M. Skowronski, M. De Graef, K. Doverspike, L.B. Rowland, D.K. Gaskill, Appl. Phys. Lett. 66 (1995) 1252.